JEMAT 2025, Vol 13, No 2, 67-77
https://doi.org/10.54987/ngcgsb21

HIBISCUS PUBLISHER

JOURNAL OF ENVIRONMENTAL MICROBIOLOGY AND TOXICOLOGY

Website: http://journal.hibiscuspublisher.com/index.php/JEMAT/index

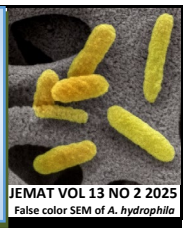

Isothermal Modeling and MOORA-Based Model Selection for Chromium Ion Adsorption by *Rhizopus nigricans*

Ismail Haruna[1,2], Mohd Ezuan Khayat[1], Nur Adeela Yasid[1], Mohd Izuan Effendi Halmi[3], Ain Aqilah Basirun[1] and M.Y. Shukor[1]*

[1]Department of Biochemistry, Faculty of Biotechnology and Biomolecular Sciences, Universiti Putra Malaysia, 43400 UPM Serdang, Selangor, Malaysia.
[2]Department of Microbiology, Faculty of Sciences, Sa'adu Zungur University, PMB 065 Itas/Gadau, Bauchi, Nigeria.
[3]Department of Land Management, Faculty of Agriculture, Universiti Putra Malaysia, 43400 UPM Serdang, Selangor, Malaysia.

*Corresponding author:
Mohd Yunus Shukor,
Department of Biochemistry,
Faculty of Biotechnology and Biomolecular Sciences,
Universiti Putra Malaysia,
43400 UPM Serdang,
Selangor,
Malaysia.
Email: mohdyunus@upm.edu.my

History

Received: 12th Aug 2025
Received in revised form: 19th Nov 2025
Accepted: 15th Dec 2025

Keywords

Rhizopus nigricans biomass
Chromium (VI) adsorption
Isothermal Modelling
MOORA ranking
Nonlinear regression

SDG Keywords

SDG 6 Clean water and sanitation
SDG 12 Responsible consumption and production
SDG 9 Industry, innovation and infrastructure

Abstract

Adsorption of hexavalent chromium (Cr(VI)) onto *Rhizopus nigricans* biomass. The Langmuir model yielded a physically justified maximum adsorption capacity, Q_{mL}, of 112.756 mg/g (95 percent confidence interval from 98.780 to 126.731 mg/g), which almost matched the experimental maximum. Despite this, the uptake capacity increases continuously with equilibrium concentration, with the final data points showing a steady upward trend rather than leveling off into a distinct plateau. This indicates that complete saturation of the binding sites has not yet been reached within the tested concentration range. Because heterogeneous isotherm models better reflected the overall equilibrium profile, model selection based just on Q_m was insufficient. The isotherm equations were directly fitted using nonlinear regression, and the model's performance was assessed using several error criteria. According to MOORA approach, Fritz-Schlunder III, Redlich-Peterson, and the Toth model are the best models overall, better than Langmuir. Despite this, all these best models failed to produce maximum adsorption capacity values near the experimental value. It is suggested that Cr(VI) biosorption by *Rhizopus nigricans* biomass included heterogeneous binding sites rather than ideal uniform monolayer adsorption. Thus, the Langmuir isotherm model initially suggested to describe this monolayer adsorption process may be inaccurate, because the uptake capacity is still actively increasing, the true maximum saturation capacity is likely higher than this maximum recorded value.This behavior is most likely impacted by the chemical variety of the fungal surface. More equilibrium points and resampling methods for parameter validation should be included in future studies.

INTRODUCTION

The cycling of chromium between its hexavalent Cr(VI) and trivalent Cr(III) forms and rapid industrial growth are the major causes of chromium pollution, which remains a major global environmental problem since chromium, particularly Cr(VI), is highly carcinogenic and toxic. Globally, chromium is primarily employed in electroplating, dye production, paper, steel fabrication, metallurgical processing, and leather tanning industries. These industries are the primary contributors to chromium pollution, resulting from the discharge of Cr(VI) due to inadequate waste management, fugitive emissions, and polluted effluents [1]. Hexavalent chromium toxicity in waterways and soils is represented by the highly mobile chromate/dichromate anionic species. Hexavalent chromium is highly mobile and can easily bioaccumulate, endangering aquatic life and human health through inhalation, ingestion, and skin contact. Inconsistent monitoring and regulatory inadequacies are the main reason for continues chromium pollution, most especially in regions close to electroplating and mining industrial zones in developing countries [2]. In Malaysia, the major sources of chromium contamination include electroplating workshops, industrial estates and leather plants. These sources result from of a combination of modern and historical pressures. Chromium contamination disproportionately affects peri-urban and rural communities by adding Cr(VI) and Cr(III) to surface waters and sediments through contaminated groundwater and downstream effluents [3]. River systems close to industrial clusters have been

found to have higher chromium concentrations in Malaysia. For maximum public health and ecosystem protection, there is a need for strong and enhanced effluent treatment, more integrated water quality management, and routine monitoring [3]. Chromium toxicity varies depending on the species. Trivalent chromium is less poisonous because of its limited solubility in water. Nevertheless, it is necessary in minimal amounts as an enzyme cofactor and becomes dangerous at high exposure levels. Conversely, Hexavalent chromium species can pass through cell membranes and have potent oxidative capacities. This species is hence extremely poisonous, mutagenic, and carcinogenic. Prolonged exposure to hexavalent chromium can cause respiratory issues, renal damage, and developmental impacts [1]. The endless need for chromium in corrosion-resistant coatings, steel alloys, and chemicals in tanning has resulted in a paradox: although chromium is required for the operation of many modern industries, excessive levels of it in the environment have serious negative effects on the environment. This issue has prompted researchers to move toward sustainable methods, such as more advanced treatment technologies and comprehensive, circular approaches, in order to control or clean up chromium contamination and waste [4].

Techniques for remediating chromium include precipitation, electrochemical treatment, chemical reduction, ion exchange, and bioremediation. Biosorption, the removal of Cr(VI) from contaminated environments by using biological materials (artificial or natural) as adsorbents, provides a number of important advantages, such as cost-effectiveness, the possibility of regenerating and reusing adsorbents, and compatibility with low-energy processes. Because of these benefits, biosorption is appealing in developing and poor nations [5–8]. The idea that biosorption is the most cost-effective and environmentally friendly method stems from a number of benefits: (1) it is economically feasible due to its low-cost feedstocks and simple processing requirements; (2) compared to physico-chemical methods, less energy is required; (3) it requires fewer chemical additives and less waste is produced; (4) there is possibility of recovering adsorbate and recycling of adsorbent, which allows for a circular use of chromium resources. Through biosorption, integrity of ecosystem is maintained, waste materials are utilized, and scalable solutions are provided in many places including Malaysia through decentralized treatment systems and pilot plants, these aligns with the UN's Sustainable Development Goals [9,10].

Dead *Rhizopus nigricans* biomass, such as *Rhizopus oryzae* and *Aspergillus niger*, have demonstrated encouraging chromium removal, especially in acidic environments where Cr(VI) species exhibit strong interactions with protonated biomass surfaces [11–14]. However, biosorption efficiency is affected by pH, particle size, biomass pretreatment, initial metal concentration, contact time, and competing ions. Thus, spent *Rhizopus nigricans* biomass should be considered a viable low-cost biosorbent; nonetheless, regeneration studies, column validation, and testing with actual industrial effluent are necessary for its practical application [15–17]. In this paper, different isotherms are used to represent the adsorption of chromium on *Rhizopus nigricans* biomass, and MOORA analysis is used to determine which model is the best.

METHODS

Data acquisition and fitting

The freeware Webplotdigitizer 2.5 was used to digitize Figure 3 data from a previously published work [18]. The program's digitizing capabilities have received praise for their dependability [19]. The data were then subjected to nonlinear regression using Curve-Expert Professional (Version 2.6.5, copyright Daniel Hyams), a curve-fitting application. The implicit equations were solved using the MATLAB software suite (Mathworks, Massachusetts, USA).

Isotherms

To avoid overfitting, the isothermal models used in this work (**Table 1**) are restricted to three-parameter models, which are displayed below.

Table 1. Mathematical models in the remodelling data.

Isotherm	p	Formula	Ref.
Henry's law	1	$q_e = HC_e$	[20]
Langmuir	2	$q_e = \frac{q_{mL} b_L C_e}{1 + b_L C_e}$	[21]
Jovanovic	2	$q_e = q_{mJ}(1 - e^{-K_J C_e})$	[22]
Freundlich	2	$q_e = K_F C_e^{\frac{1}{n_F}}$	[23]
Dubinin-Radushkevich[a]	2	Incorrect form $q_e = q_{mDR} exp\left\{-K_{DR}\left[RTln\left(1+\frac{1}{C_e}\right)\right]^2\right\}$	[24,25]
		correct form $q_e = q_{mDR} exp\left\{-K_{DR}\left[RTln\left(\left(\frac{C_s}{C_e}\right)\right)\right]^2\right\}$	[26,27]
Koble-Corrigan[c]	3	$q_e = \frac{AC_e^n}{1 + BC_e^n}$	[28]
Temkin[a]	3	$q_e = \frac{RT}{b_T}\{ln(a_T C_e)\}$	[29,30]
Redlich-Peterson	3	$q_e = \frac{K_{RP1} C_e}{1 + K_{RP2} C_e^{\beta_{RP}}}$	[31]
Sips[c]	3	$q_e = \frac{K_s q_{mS} C_e^{\frac{1}{n_S}}}{1 + K_s C_e^{\frac{1}{n_S}}}$	[32]
Toth	3	$q_e = \frac{q_{mT} C_e}{\left(K_T + C_e^{n_T}\right)^{n_T}}$	[33]
Hill[c]	3	$q_e = \frac{q_{mH} C_e^{n_H}}{K_H + C_e^{n_H}}$	[34]
BET	3	$q_e = \frac{q_{mBET} \alpha_{BET} C_e}{(1 - \beta_{BET} C_e)(1 - \beta_{BET} C_e + \alpha_{BET} C_e)}$	[35]
Vieth-Sladek	3	$q_e = \frac{q_{mVS} b_{VS} C_e}{(1 + b_{VS} C_e)^{n_{VS}}}$	[36]
Brouers–Sotolongo	3	$q_e = q_{mBS}\left[1 - \left(1 + (0.5)\left(\frac{t}{\tau}\right)^{\alpha}\right)^{-2}\right]$	[37–39]
Fritz-Schlunder-III	3	$q_e = \frac{q_{mFS} K_{FS} C_e}{1 + K_{FS} C_e^{n_{FS}}}$	[40]
Fowler-Guggenheim[a,b]	3	$q_e = q_{mFG} \frac{K_L C_e e^{\frac{\alpha q_e}{q_{mFG}}}}{1 + K_L C_e e^{\frac{\alpha q_e}{q_{mFG}}}}$	[41]
Moreau	3	$q_e = q_{mM} \frac{bC_e + lb^2 C_e^{\,2}}{1 + 2bC_e + lb^2 C_e^{\,2}}$	[42]
Unilan	3	$q_e = \frac{q_{mU}}{2b_U} ln\left(\frac{a_U + C_e e^{b_U}}{a_U + C_e e^{-b_U}}\right)$	

Note
[a]Models that include ln(C_e), implicit equation or any logarithmic function involving C_e will fail or produce NaN (undefined) results when $C_e = 0$. Therefore, data points where $C_e = 0$ should be excluded from the analysis.
[b]Implicit equation or function.
[c]The Hill, Liu (omitted), Sips, and Koble–Corrigan isotherm models will be presented in their traditional forms to preserve their historical context and conceptual distinctions, despite their underlying equality [43,44].

Statistical analysis

Statistical discriminatory or error function tests utilized in this study include corrected Akaike Information Criterion (AICc) [45,46], root-mean-squared error (RMSE), adjusted coefficient of determination (R^2) [47], Bias Factor (BF), Accuracy Factor (AF) [48], Marquardt's percent standard deviation (MPSD) [49–51], and Bayesian Information Criterion [52]. O*bi* and P*di* are the

expected and observed values, n is the total number of observations, and p is the total number of model parameters [53].

RMSE was calculated using the following formula;

$$RMSE = \sqrt{\frac{\sum_{i=1}^{n}(Pd_i - Ob_i)^2}{n-p}} \quad \text{(Eqn. 1)}$$

BF and AF were calculated using the following formula;

$$Bias\ factor = 10\left(\sum_{i=1}^{n} log\frac{(Pd_i/Ob_i)}{n}\right) \quad \text{(Eqn. 2)}$$

$$Accuracy\ factor = 10\left(\sum_{i=1}^{n} log\frac{|(Pd_i/Ob_i)|}{n}\right) \quad \text{(Eqn. 3)}$$

AICc was calculated using the following formula;

$$AICc = 2p + n\ln\left(\frac{RSS}{n}\right) + \frac{2(p+1)+2(p+2)}{n-p-2} \quad \text{(Eqn. 4)}$$

BIC was calculated using the following formula;

$$BIC = n\ln\left(\frac{RSS}{n}\right) + k\ln(n) \quad \text{(Eqn. 5)}$$

HQC was calculated using the following formula;

$$HQC = nIn\left(\frac{RSS}{n}\right) + 2k\ln(\ln n) \quad \text{(Eqn. 6)}$$

Adjusted coefficient of determination (R^2) was calculated using the following formula;

$$Adjusted\ (R^2) = 1 - \frac{RMS}{S_Y^2} \quad \text{(Eqn. 7)}$$

$$Adjusted\ (R^2) = 1 - \frac{(1-R^2)(n-1)}{(n-p-1)} \quad \text{(Eqn. 8)}$$

MPSD was calculated using the following formula;

$$MPSD = 100\sqrt{\frac{1}{n-p}\sum_{i=1}^{n}\left(\frac{Ob_i - Pd_i}{Ob_i}\right)^2} \quad \text{(Eqn. 9)}$$

Application of Multiobjective Optimization by Ratio Analysis (MOORA) in Modeling

Since the best models frequently have a mixture of error function superiority, the Multiobjective Optimization by Ratio Analysis (MOORA) was used for multi-criteria decision-making (MCDM) in the modeling exercise. By concurrently assessing several performance criteria, this method makes it easier to choose the best model [54,55]. To achieve comparability across various performance indicators, the initial step in the process is to normalize the decision matrix. After that, the choice matrix was normalized. The following equation must be used for normalization because these measurements may have different units and magnitudes:

$$X'_{ij} = \frac{X_{ij}}{\sqrt{\sum_{i=1}^{n} X_{ij}^2}} \quad \text{(Eqn. 10)}$$

Where X_{ij} is the original value of the j^{th} metric for the i^{th} model, and X'_{ij} is the normalized value**.**

Ratio System Analysis

A ratio system approach was then used to aggregate the normalized values. The following formula was used to deduct non-beneficial criteria (the remaining error functions) or those that should be minimized from advantageous criteria (those that should be maximized, adjR^2).

$$Y_i = \sum_{beneficial} X'_{ij} - \sum_{non-beneficial} X'_{ij} \quad \text{(Eqn. 11)}$$

Where Y_i is the final score for the i^{th} model

It is advised to include weighted ratios in the analysis when some criteria were judged to be more important than others. Since there is currently no consensus in the literature over which of the error functions mentioned above should take precedence over the others, the recommendation to incorporate Weighted Ratios is not implemented. Ranking models according to their combined performance scores is the last stage. Better performance was reflected by higher scores. According to the specified decision criteria, the model with the highest value was deemed the best. This approach made it possible to compare kinetic models objectively and methodically, making it easier to determine which model performed the best while taking into account several performance criteria at once.

RESULTS AND DISCUSSION

Nonlinear regression was used to apply various models to the equilibrium data of [18]. The experimental isotherm profile (**Fig. 1**) demonstrated that when the equilibrium concentration, C_e, increased, so did the *Rhizopus nigricans* biomass's uptake of Cr(VI). The adsorption capacity q_e increased dramatically from about 25 to 65 mg Cr/g at low C_e, suggesting a high initial affinity between Cr(VI) species and easily accessible binding sites on the *Rhizopus nigricans* biomass surface. At the highest tested concentration, q_e grew more gradually as C_e increased, reaching about 117 mg Cr/g. A fully horizontal plateau was not clearly created, despite the curve's inclination toward saturation, indicating that the true maximum adsorption capacity may not have been entirely reached within the examined range.

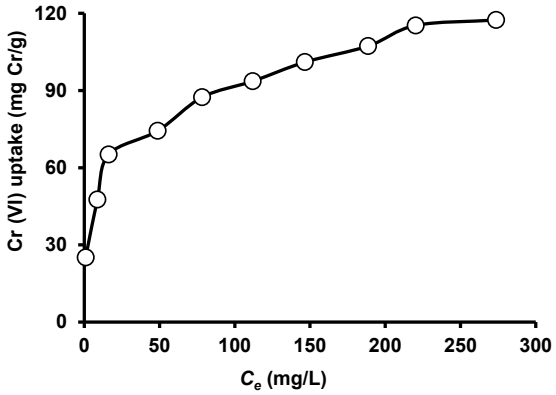

Fig. 1. Equilibrium adsorption of chromium to *Rhizopus nigricans* biomass raw data extracted using Webplot.

The adsorption behavior was better explained by heterogeneous and multi-parameter models than by more straightforward two-parameter equations, according to nonlinear isotherm fitting. Toth was ranked as the best model by MOORA, followed by Fritz-Schlunder III, Redlich-Peterson, Brouers-Sotolongo, and Sips, with Hill and Sips sharing the same position. Strong adsorption on a heterogeneous *Rhizopus nigricans* biomass surface with a variety of binding groups, including hydroxyl, carboxyl, phosphate, amine, and amide groups, is suggested by the good performance of Toth, Fritz-Schlunder III, and Redlich-Peterson [18,15–17]. Conversely, Temkin, Jovanovic, BET, Koble-Carrigan, and Henry performed worse, while Langmuir only came in at number twelve. Consequently, even though the curve indicated partial saturation, an ideal homogeneous monolayer model was unable to explain the adsorption process. Overall, Toth is the best model for Cr(VI) biosorption by the *Rhizopus nigricans* biomass, according to the MOORA data.

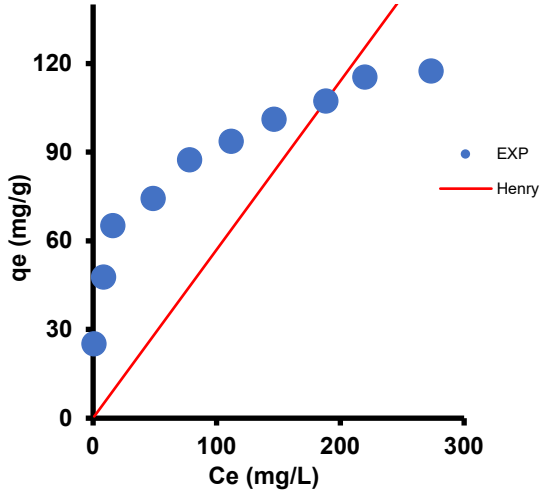

Fig. 2. Cr (VI) adsorption onto *Rhizopus nigricans* biomass modelled using the Henry model.

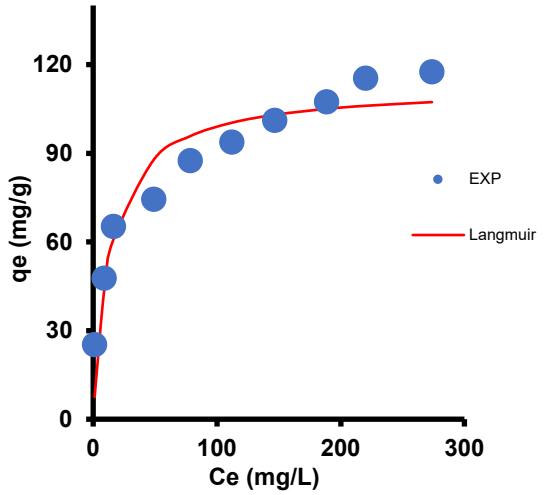

Fig. 3. Cr (VI) adsorption onto *Rhizopus nigricans* biomass modelled using the Langmuir isotherm model.

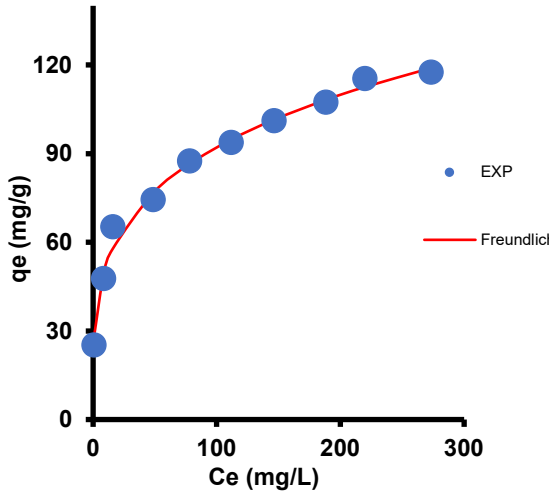

Fig. 4. Cr (VI) adsorption onto *Rhizopus nigricans* biomass modelled using the Freundlich isotherm model.

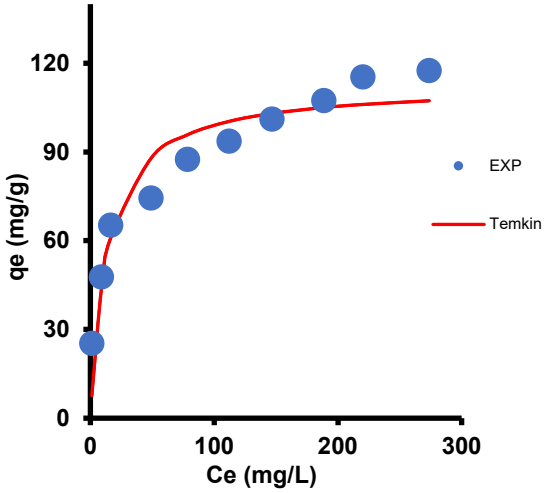

Fig. 5. Cr (VI) adsorption onto *Rhizopus nigricans* biomass modelled using the Temkin isotherm model.

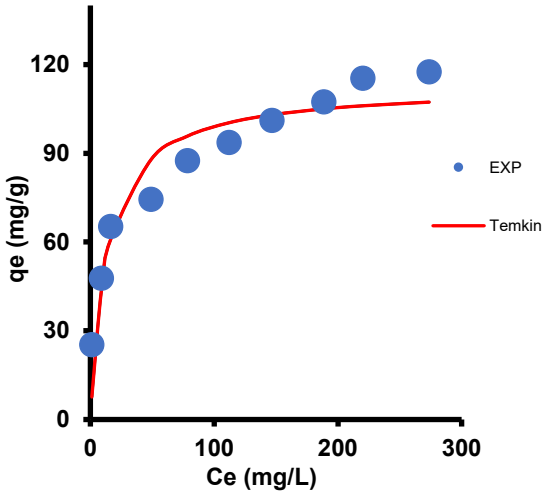

Fig. 6. Cr (VI) adsorption onto *Rhizopus nigricans* biomass modelled using the Koble-Corrigan isotherm model.

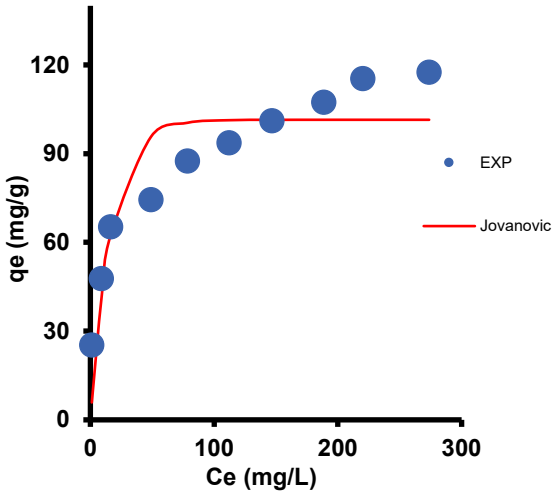

Fig. 7. Cr (VI) adsorption onto *Rhizopus nigricans* biomass modelled using the Jovanovic isotherm model.

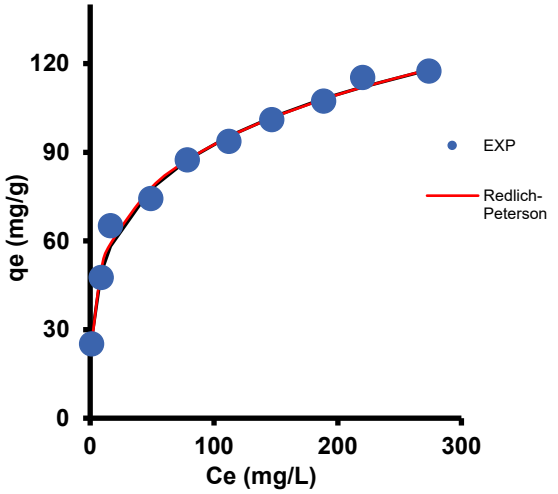

Fig. 8. Cr (VI) adsorption onto *Rhizopus nigricans* biomass modelled using the Redlich-Peterson isotherm model.

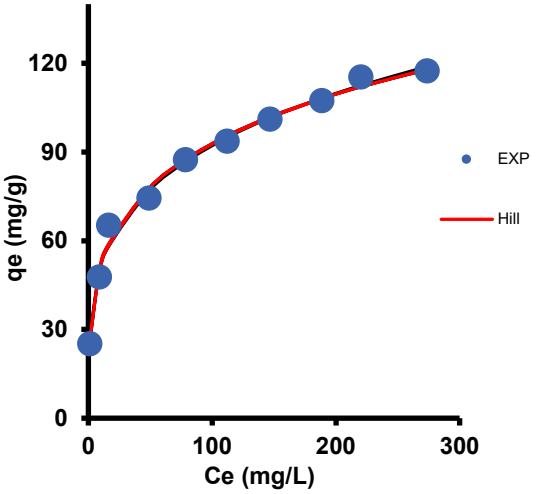

Fig. 11. Cr (VI) adsorption onto *Rhizopus nigricans* biomass modelled using the Hill isotherm model.

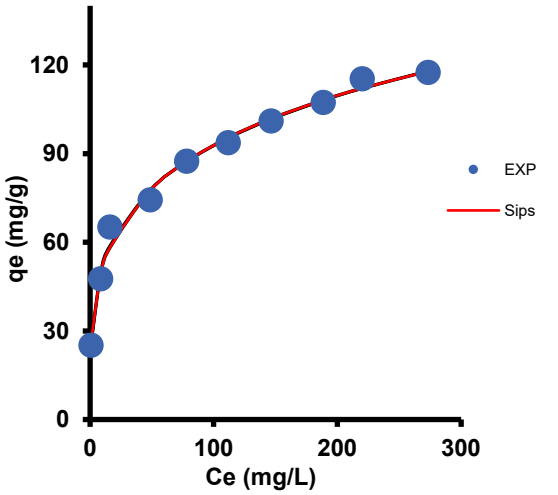

Fig. 9. Cr (VI) adsorption onto *Rhizopus nigricans* biomass modelled using the Sips isotherm model.

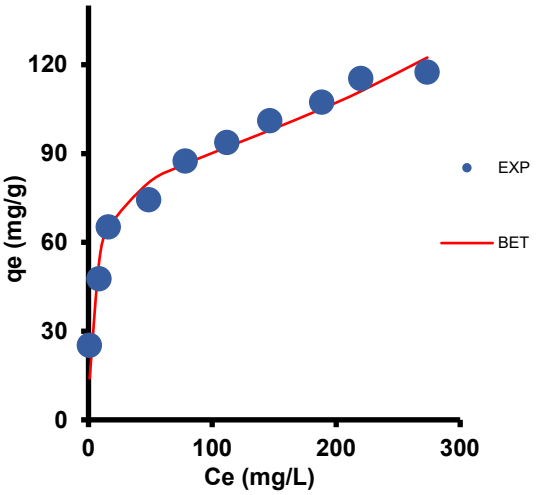

Fig. 12. Cr (VI) adsorption onto *Rhizopus nigricans* biomass modelled using the BET isotherm model.

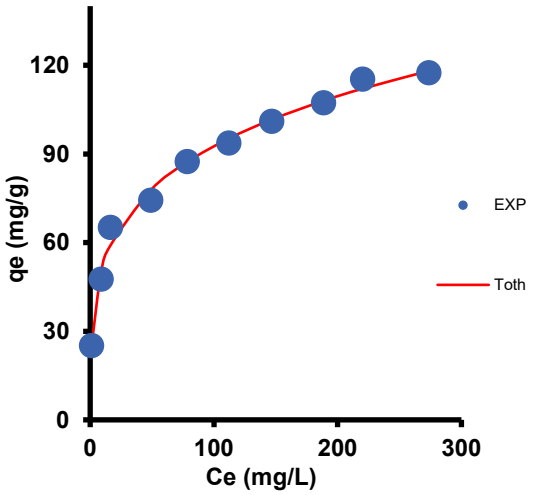

Fig. 10. Cr (VI) adsorption onto *Rhizopus nigricans* biomass modelled using the Toth isotherm model.

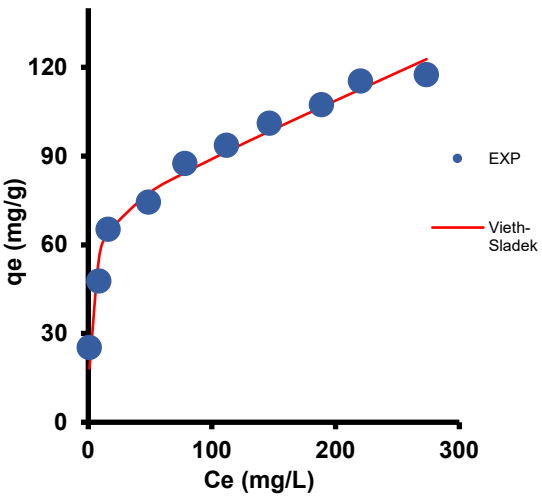

Fig. 13. Cr (VI) adsorption onto *Rhizopus nigricans* biomass modelled using the Vieth-Sladek isotherm model.

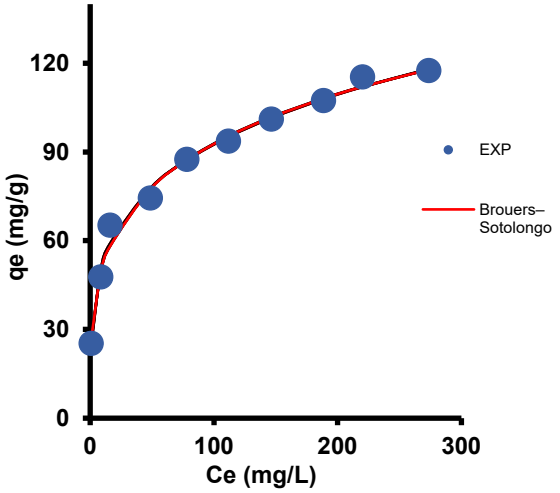

Fig. 14. Cr (VI) adsorption onto *Rhizopus nigricans* biomass modelled using the Brouers-Sotolongo isotherm model.

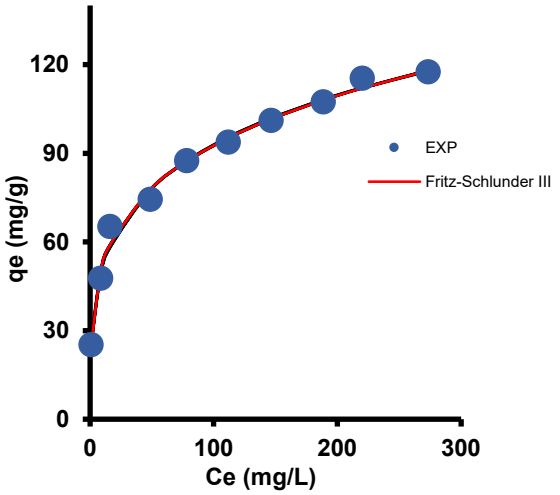

Fig. 15. Cr (VI) adsorption onto *Rhizopus nigricans* biomass modelled using the Fritz-Schlunder III isotherm model.

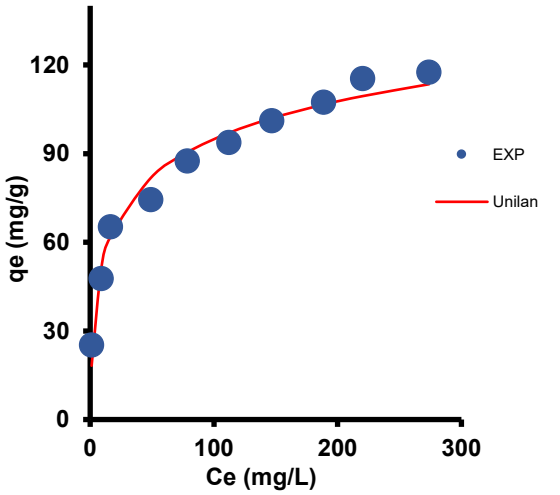

Fig. 16. Cr (VI) adsorption onto *Rhizopus nigricans* biomass modelled using the Unilan isotherm model.

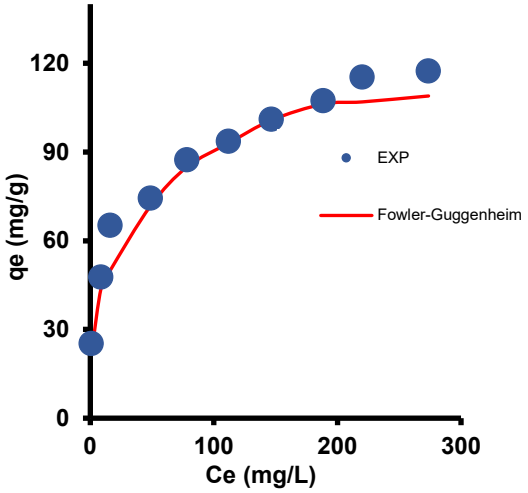

Fig. 17. Cr (VI) adsorption onto *Rhizopus nigricans* biomass modelled using the Moreau isotherm model.

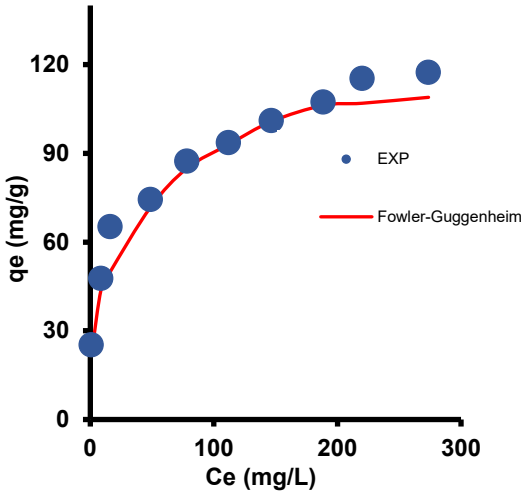

Fig. 18. Cr (VI) adsorption onto *Rhizopus nigricans* biomass modelled using the Fowler-Guggenheim isotherm model.

Spent *Rhizopus nigricans* biomass is a desirable biosorbent for removing metal ions from aqueous effluents because it is frequently available as a waste by-product from fermentation or enzyme production operations, and it is also abundant and inexpensive. Spent or dead *Rhizopus nigricans* biomass can be employed in a wider range of environmental conditions, no nutrients requirement, and is less impacted by metal toxicity than living biomass. The biosorption capacity of *Rhizopus nigricans* biomass is primarily linked to its cell-wall constituents such chitin, glucans, proteins, and polysaccharides, which offer hydroxyl, carboxyl, phosphate, amine, and amide functional groups for metal binding. These groups can eliminate Cr(VI), Pb(II), Cd(II), Cu(II), Ni(II), and Zn(II) through complexation, ion exchange, surface precipitation, electrostatic attraction, and potential reduction of Cr(VI) to the less hazardous Cr(III).

Table 2. Error function analysis for the fitting of the isotherm of Cr (VI) adsorption onto *Rhizopus nigricans* biomass.

	Model	*p*	MPSD	RMSE	R^2	adR^2	AICc	BIC	HQC	BF	AF
1	Henry	1	197.32	37.011	0.54	0.480	78.885	73.47	72.84	0.916	1.175
2	Langmuir	2	26.58	10.230	0.92	0.894	58.275	48.88	47.61	0.999	1.038
3	Freundlich	2	77.34	3.256	0.99	0.986	35.376	25.98	24.71	1.000	1.007
4	Temkin	3	29.12	10.936	0.92	0.877	66.274	51.18	49.28	0.999	1.038
5	Koble-Carrigan	2	315.29	3.140	0.96	0.95	34.651	25.26	23.99	1.001	1.007
6	Jovanovic	2	10.56	14.126	0.84	0.801	64.728	55.33	54.06	0.989	1.057
7	Redlich-Peterson	3	9.77	3.165	0.99	0.987	41.476	26.38	24.48	1.000	1.006
8	Sips	3	21.51	3.356	0.99	0.985	42.651	27.56	25.66	1.001	1.007
9	Toth	3	9.72	3.154	0.99	0.987	41.409	26.32	24.41	1.000	1.006
10	Hill	3	21.51	3.356	0.99	0.985	42.651	27.56	25.66	1.001	1.007
11	Khan	3	9.94	84.942	0.03	-0.449	######	92.18	90.28	1.414	1.414
12	BET	3	173.39	6.067	0.97	0.958	54.489	39.40	37.49	0.992	1.016
13	Vieth-Sladek	3	9.94	5.044	0.98	0.969	50.797	35.71	33.80	0.993	1.016
14	Radke-Prausnitz	3	9.94	84.942	0.03	-0.449	######	92.18	90.28	1.414	1.414
15	Brouers–Sotolongo	3	11.16	3.366	0.99	0.985	42.706	27.61	25.71	1.001	1.007
16	Fritz-Schlunder III	3	9.78	3.164	0.99	0.987	41.473	26.38	24.48	1.000	1.006
17	Unilan	3	29.61	5.302	0.98	0.965	51.796	36.70	34.80	0.999	1.017
18	Fowler-Guggenheim	3	54.58	4.395	0.98	0.976	48.043	32.95	31.05	0.998	0.998
19	Moreau	3	39.34	7.641	0.95	0.923	59.103	44.01	42.11	0.985	0.985

Note:
RMSE Root mean Square Error
adR^2 Adjusted Coefficient of determination
p no of parameters
AF Accuracy factor
BF Bias factor
BIC Bayesian Information Criterion
AICc Adjusted Akaike Information Criterion
HQC Hannan–Quinn information criterion

Table 3. Ranking of isothermal models based on MOORA.

No	Model	MOORA Score	Rank
1	Toth	0.05884	1
2	Fritz-Schlunder III	0.05775	2
3	Redlich-Peterson	0.05771	3
4	Brouers–Sotolongo	0.03546	4
5	Sips	0.01214	5
6	Hill	0.01214	5
7	Freundlich	-0.07768	7
8	Vieth-Sladek	-0.09553	8
9	Fowler-Guggenheim	-0.14920	9
10	Unilan	-0.15766	10
11	Moreau	-0.31211	11
12	Langmuir	-0.37354	12
13	Temkin	-0.43939	13
14	Jovanovic	-0.50297	14
15	BET	-0.54057	15
16	Koble-Carrigan	-0.63923	16
17	Henry	-1.55453	17

Table 4. Isothermal models' constants for Cr (VI) adsorption onto *Rhizopus nigricans* biomass.

Model	Para-meter	Unit	Value	95% CI
Langmuir	Qm_S	(mg/g)	112.756	98.780 to 126.731
	k_L	(L/mg)	0.072	0.022 to 0.123
Redlich-Petersen	k_{RP1}	(L/g)	133.188	-149.374 to 415.749
	k_{RP2})	(L/mg)/g	4.248	-5.536 to 14.033
	B_{RP}	dimensionless	0.763	0.719 to 0.808
Toth	q_{mT}	(mg g^{-1})	30.94	24.473 to 37.410
	K_T	$(mg/L)^{nT}$	0.26	-0.330 to 0.850
	n_T	dimensionless	0.87	0.849 to 0.896
Fritz-Schlunder III	q_{mFS}	(mg g^{-1})	31.350	24.124 to 38.576
	K_{FS}	dimensionless	4.248	-5.534 to 14.031
	nF_S	dimensionless	0.763	0.719 to 0.808
Brouers-Sotolongo isotherm	qm_{BS}	mg g^{-1}	311.586	-473.516 to 1096.688
	K_{BS}	$mg^{-1/nBS}$ $L^{1/nBS}$	0.091	0.132 to 0.314)
	n_{BS}	dimensionless	3.391	1.824 to 4.958
Hill isotherm	q_{mH}	mg g^{-1}	493.692	-853.999 to 1841.382
	n_H	dimensionless	0.302	0.145 to 0.459
	K_H	dimensionless	17.330	-29.440 to 64.100
Sips	*qmS*	mg g-1	493.135	-848.289 to 1834.559
	KS	(L mg-1)ns	0.058	-0.097 to 0.213
	nS	dimensionless	3.314	1.589 to 5.039

The Langmuir model calculated a maximum adsorption capacity, Q_{mL}, of 112.756 mg/g with a standard error of 6.060 and a 95 percent confidence interval of 98.780 to 126.731 mg/g based on the adjusted Langmuir parameters. The Langmuir model gave a physically reasonable estimate of the upper adsorption capacity within the examined concentration range, as evidenced by the fact that this value is near the greatest experimentally observed adsorption capacity. With a 95 percent confidence interval of 0.022 to 0.123 L/mg, the Langmuir affinity constant, K_L, was 0.072 L/mg, indicating a moderate affinity between Cr(VI) species and the *Rhizopus nigricans* biomass surface.

However, the Langmuir model should not be immediately regarded as the best model based only on its capacity estimate, even though the Q_{mL} value is physically feasible. The Toth model provided the best overall fit, according to the MOORA ranking, followed by Fritz-Schlunder III and Redlich-Peterson. This should be expected because fungus has various functional groups, such as hydroxyl, carboxyl, phosphate, amine, and amide groups, in its cells that have chemical binding sites. This implies that an exact description of the entire equilibrium profile is provided by the models that account for surface heterogeneity and non-ideal adsorption.

The maximum computed chromium adsorption capacity of the Toth model q_{mT} was 30.94 mg/g with an interval of 24.473 to 37.410 mg/g at 95 percent confidence. Despite having a lower value than the Langmuir Q_{mL}, the Toth model was ranked best according to the total model-selection criteria. With a narrow 95 percent confidence interval of 0.849 to 0.896, its heterogeneity exponent, n_T, was 0.87, showing a shift from perfect homogenous Langmuir-type adsorption. Consequently, the Toth model's ability to explain the equilibrium data is its major strength.

The Fritz-Schlunder III model provided a similar calculated maximum equilibrium adsorption capacity, q_{mFS}, of 31.350 mg/g with a 95 percent confidence interval of 24.124 to 38.576 mg/g. With a confidence interval of 0.719 to 0.808 and exponent n_{FS} of 0.763, non-ideal adsorption behavior is demonstrated again. The affinity-related parameter K_{FS}, however, displayed a large confidence range that crossed zero, suggesting a lower level of

precision in this parameter estimation. Fritz-Schlunder III may therefore be helpful as an empirical fitting model, although care should be used when interpreting its parameters. With a 95 percent confidence interval of 0.719 to 0.808 and an estimated B_{RP} of 0.763, the Redlich-Peterson model likewise demonstrated heterogeneous adsorption. The model did not reduce to the Langmuir form and did not produce a finite theoretical Q_m because B_{RP} was obviously below unity. Rather, the experimental concentration range continues to influence the expected adsorption capacity. Furthermore, there was significant uncertainty in these fitted constants as k_{RP1} and k_{RP2} displayed large confidence ranges that crossed zero.

The three other models, namely Brouers–Sotolongo, Hill and Sips, showed higher estimated maximum adsorption values but with a wide range of confidence intervals, and in some cases, extended into negative lower limits. This wide range indicates that the maximum-capacity parameters were inappropriately covered by the available data, with the most likely reason being insufficient high-concentration data, as can be seen in **Fig. 1**, with no clear definition of a saturation plateau. The results imply that Cr(VI) adsorption onto the *Rhizopus nigricans* biomass was best explained by adsorption to a heterogeneous system. Due to this, the estimated Qm values from Brouers–Sotolongo, Hill and Sips are not true theoretical maximum adsorption capacities but is likely model-dependent apparent capacities. More data are needed to describe the plateau region.

Overall, the adjusted Langmuir parameters demonstrate that Langmuir generated a reasonable and tightly controlled Q_{mL} of roughly 113 mg/g. Toth, Fritz-Schlunder III, and Redlich-Peterson's higher MOORA ranking, however, indicates that Cr(VI) adsorption onto the *Rhizopus nigricans* biomass was more accurately characterized as a heterogeneous process than as ideal monolayer adsorption on a uniform surface. Therefore, Langmuir may be useful for reporting an apparent maximum adsorption capacity, whereas Toth is more appropriate for describing the overall equilibrium behaviour.

In addition to standardizing performance ratings across criteria, MOORA is known for its computational efficiency and simplicity, which eliminates the need for complex pairwise comparisons or distance calculations. By managing criteria with different scales and units through organized normalization, MOORA allows for quick and easy evaluation. MCDM has been effectively and extensively applied in a number of model ranking tasks, such as the evaluation of Software Reliability Growth Models (SRGMs) [56]. Nevertheless, it is still rarely used in the selection of adsorption models [44]. As previously indicated, a major drawback of nonlinear modeling is it inability to adequately represent adsorption behavior of small datasets, like the eight data points utilized in this work. Instead of recognizing authentic adsorption patterns, an insufficient dataset increases the chances of recording random noise. This usually results in poor parameter estimation and overfitting of adsorption models, as well as a wrong comprehension of adsorption mechanisms. Small datasets reduce statistical power and widen confidence intervals. To solve issues related to small datasets and gain additional understanding of adsorption behavior, resampling techniques like bootstrapping, Monte Carlo simulations, and sensitivity analysis can be used to improve model resilience [57].

Toth

The Toth isotherm, a three-parameter model that preserves the appropriate low- and high-concentration limits, describes adsorption on heterogenically energetic surfaces. Langmuir isotherm is provided by n_T value approaching unity in the equation, where $n_T \rightarrow 1$ indicates stronger homogeneity. It retains physical meaning over wide ranges and reproduces Henry's rule for low C_e values. In several studies, the Toth isotherm usually outperforms Sips and Langmuir in the adsorption of organics and dyes, suggesting the model's ability to manage broad site-energy distributions and, at the same time, maintain the monolayer capacity approach [58,59].

Redlich–Peterson model

The Redlich-Peterson (RP) isotherm is a flexible three-parameter equation that is helpful for heterogeneous surfaces because it interpolates between Langmuir and Freundlich behavior; in the model, the heterogeneity exponent γ ranges from 0 to 1; when γ = 1, the RP isotherm decreases to Langmuir with an apparent monolayer capacity. However, it adheres to Henry's law at low Ce. Nonlinear regression should be carried out over the linearized forms because of the association between its two parameters. The model is highly recommended and acclaimed as a benchmark for the three-parameter model [60–65]. The Redlich-Peterson model does not yield a finite theoretical Q_m because the fitted exponent, BRP, was 0.763 rather than 1.0. The predicted capacity is still variable on concentration since the equation does not converge to a stable saturation plateau when BRP < 1. Within the studied experimental range, the model predicted an apparent maximum uptake of approximately 118 mg/g at the highest equilibrium concentration, which is consistent with the observed upper qe region. Consequently, rather than serving as a source of a conclusive monolayer Q_m, the Redlich-Peterson finding should be seen as an empirical description of heterogeneous adsorption [31,61,66].

Langmuir isotherm

The Langmuir isotherm characterizes monolayer adsorption of an adsorbate onto a homogenous adsorbent surface, which only happens when the adsorbent has a uniform structure. In the model, all adsorption sites are identical and have the same energy [67]. Although the isotherm model and Henry's law are different, their underlying ideas are similar. The concept of monolayer coverage is supported by the theory that once a single layer of adsorbate molecules completely covers the surface, no more adsorption may take place at those locations [61]. The model has proven to be the most effective in simulating equilibrium chromium adsorption to adsorbents [68–81].

Fritz-Schlunder III Model

Multilayer adsorption and interactions between adsorbed molecules on heterogeneous surfaces are explicitly described by the Fritz-Schlunder III model. With q_{mFS}, K_{FS}, and nF_S as constants that represent the maximal adsorption capacity, the affinity of the binding sites, and the interactions between adsorbed molecules, respectively, this model takes into account the potential for multilayer adsorption at higher concentrations. Compared to the Langmuir model, the model seeks to offer a more adaptable and universal approach to adsorption isotherms that can explain a greater variety of adsorption processes. Multilayer adsorption and interactions between adsorbed molecules are explicitly taken into account by the Fritz-Schlunder III model, which incorporates a quadratic term in the denominator. The Fritz-Schlunder III model is particularly useful for systems where multilayer adsorption and molecule-molecule interactions are important.

The proposed binding sites and interaction mechanisms for Cr(VI) oxyanions on fungal biomass cell wall shows a multitude of functional groups interacting with the chromate anions (**Fig. 19**). In aqueous system, Cr(VI) occurs as chromate, hydrogen chromate, or dichromate species depending on solution pH and

the chromium concentration. The interactions of these oxyanions with fungal cell wall components such as chitin/chitosan, glucans, proteins, and melanin-like materials occur through several possible mechanisms. This mechanism include electrostatic attraction to protonated amino groups, hydrogen bonding with hydroxyl and amide groups, surface complexation with carboxyl or ion exchange, phosphate, and sulfate groups. In addition, physical adsorption within the heterogeneous cell wall matrixmay occur. The following diagram highlights the possible Cr(VI) biosorption through the combined contribution of multiple functional groups. These dominant mechanism depends on pH, Cr(VI) speciation, biomass surface charge, and experimental conditions.

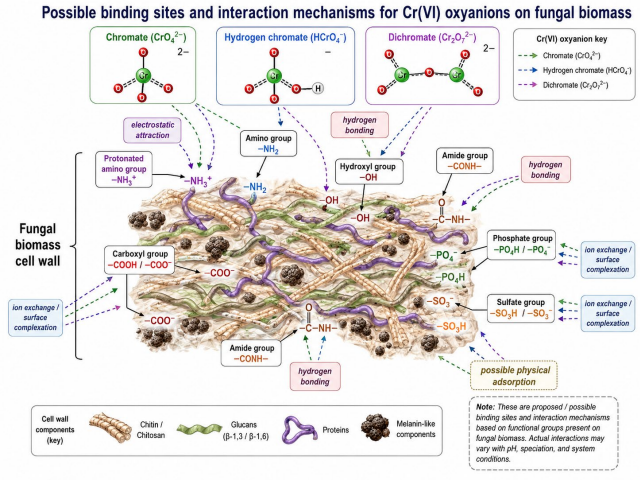

Fig. 19. Proposed Cr(VI) oxyanion binding to fungal biomass via electrostatic attraction, hydrogen bonding, ion exchange, surface complexation, and physical adsorption involving amino, hydroxyl, carboxyl, amide, phosphate, sulfate, and cell wall components (Illustration generated with the assistance of ChatGPT (OpenAI) based on the authors' instructions).

CONCLUSION

Cr(VI) adsorption onto *Rhizopus nigricans* biomass was better characterized by a heterogeneous biosorption process with partial Langmuir-like saturation behavior, according to nonlinear modeling. With a 95 percent confidence interval of 98.780 to 126.731 mg/g, the corrected Langmuir model produced a physically meaningful Q_{mL} of 112.756 mg/g, which was near the maximum experimental adsorption capacity of roughly 117 mg/g. This implies that Langmuir can still be used to determine the apparent maximal uptake capacity. However, the MOORA assessment showed that heterogeneous isotherms offered a better explanation for the whole equilibrium profile, with the Toth model being the best overall model, followed by Fritz-Schlunder III and Redlich-Peterson. This is in line with the complex chemical structure of *Rhizopus nigricans* biomass, which contains many functional groups for metal binding. Even if MOORA and nonlinear regression improved model selection, the limited dataset remains a disadvantage. Future studies should incorporate additional equilibrium points, and more reliable parameter validation should be achieved by bootstrapping or Monte Carlo simulation.

DECLARATION OF COMPETING INTEREST

The authors declare no competing financial interests or personal relationships.

ACKNOWLEDGEMENT

This research is funded by Universiti Putra Malaysia Inisiatif Putra Siswazah Grant, with a reference to GP-IPS/2024/GP-IPS/9785100 and the essential facilities were provided by UDRP Bioremediation and Conservation, Universiti Putra Malaysia.

AUTHORS' CONTRIBUTION

I.H. contributed to conceptualization, methodology, analysis, and writing the original draft. M.E.K. was involved in methodology, investigation, and data analysis. N.A.Y. contributed to investigation, resources, and data collection. A.A.B. participated in investigation, resources, and image generation. M.Y.S. contributed to methodology, validation, and writing review and editing.

DATA AVAILABILITY STATEMENT

Data available on request

AI USAGE DECLARATION

During the preparation of this work, the authors used generative AI technologies solely for language editing and refinement. All of the authors reviewed and edited the content. The authors take full responsibility for the final content of the publication.

REFERENCES

1. Tumolo M, Ancona V, De Paola D, Losacco D, Campanale C, Massarelli C, et al. Chromium Pollution in European Water, Sources, Health Risk, and Remediation Strategies: An Overview. Int J Environ Res Public Health. 2020 Jan;17(15):5438. doi:10.3390/ijerph17155438
2. Mohammadpour A, Gharehchahi E, Gharaghani MA, Shahsavani E, Golaki M, Berndtsson R, et al. Assessment of drinking water quality and identifying pollution sources in a chromite mining region. J Hazard Mater. 2024 Dec 5;480:136050. doi:10.1016/j.jhazmat.2024.136050
3. Idriss AA, Ahmad AK. Heavy Metals Nickel and Chromium in Sediments in the Juru River, Penang, Malaysia. J Environ Prot. 2013 Nov 8;2013. doi:10.4236/jep.2013.411144
4. Madhavi V, Reddy AVB, Reddy KG, Madhavi G, Prasad TNVKV. An overview on research trends in remediation of chromium. Res J Recent Sci. 2013;2(1):71–83.
5. Chaudhuri M, Azizan NKB. Adsorptive Removal of Chromium(VI) from Aqueous Solution by an Agricultural Waste-Based Activated Carbon. Water Air Soil Pollut. 2012 May 1;223(4):1765–71. doi:10.1007/s11270-011-0981-8
6. Amir A, Rahim R, Abdul-Talib S. Removal of Chromium Hexavalent Using Agriculture Waste. Int J Environ Sci Dev. 2017 Jan 1;8:260–3. doi:10.18178/ijesd.2017.8.4.959
7. Hanafiah SFM, Salleh NFM, Ghafar NA, Shukri NM, Kamarudin NHN, Hapani M, et al. Efficiency of Coconut Husk as Agricultural Adsorbent in Removal of Chromium and Nickel Ions from Aqueous Solution. IOP Conf Ser Earth Environ Sci. 2020 Dec;596(1):012048. doi:10.1088/1755-1315/596/1/012048
8. Konradt N, Dillmann S, Becker J, Schroden D, Rohns HP, Wagner C, et al. Removal of Chromium Species from Low-Contaminated Raw Water by Different Drinking Water Treatment Processes. Water. 2023 Jan;15(3):3. doi:10.3390/w15030516
9. Singh VP, Godara P, Srivastava A. Sustainable microalgal bioremediation of heavy metals and dyes from synthetic wastewater: Progressing towards United Nations Sustainable Development Goals. Waste Manag Bull. 2024 Dec 1;2(4):123–35. doi:10.1016/j.wmb.2024.10.005
10. Meftah S, Meftah K, Drissi M, Radah I, Malous K, Amahrous A, et al. Heavy metal polluted water: Effects and sustainable treatment solutions using bio-adsorbents aligned with the SDGs. Discov Sustain. 2025 Feb 25;6(1):137. doi:10.1007/s43621-025-00895-6

11. Cervantes C, Campos-García J, Devars S, Gutiérrez-Corona F, Loza-Tavera H, Torres-Guzmán JC, et al. Interactions of chromium with microorganisms and plants. FEMS Microbiol Rev. 2001;25(3):335–47. doi:10.1016/S0168-6445(01)00057-2
12. Khambhaty Y, Mody K, Basha S, Jha B. Kinetics, equilibrium and thermodynamic studies on biosorption of hexavalent chromium by dead fungal biomass of marine *Aspergillus niger*. Chem Eng J. 2009 Jan 1;145(3):489–95. doi:10.1016/j.cej.2008.05.002
13. Zinicovscaia I, Safonov AV, Khijniak TV. Biosorption of hexavalent chromium and uranium by bacteria, microalga, and fungi [Internet]. 2017. 333–359 p. Available from: https://www.scopus.com/inward/record.uri?eid=2-s2.0-85058593571&doi=10.1201%2f9781315366029&partnerID=40&md5=867e0799806912213ce90b932df7caf9 doi:10.1201/9781315366029
14. Pandey K, Saharan B, Kumar R, Jabborova D, Duhan J. Modern-Day Green Strategies for the Removal of Chromium from Wastewater. J Xenobiotics. 2024 Nov 3;14. doi:https://doi.org/10.3390/jox14040089
15. Park D, Yun YS, Park JM. Use of dead fungal biomass for the detoxification of hexavalent chromium: screening and kinetics. Process Biochem. 2005 Jun 1;40(7):2559–65. doi:10.1016/j.procbio.2004.12.002
16. Mungasavalli DP, Viraraghavan T, Jin YC. Biosorption of chromium from aqueous solutions by pretreated *Aspergillus niger*: Batch and column studies. Colloids Surf Physicochem Eng Asp. 2007 Jul 5;301(1):214–23. doi:10.1016/j.colsurfa.2006.12.060
17. Beig SUR, Shah SA. Biosorption of Cr (VI) by acid-modified based-waste fungal biomass from Calocybe indica fruiting bodies production. Int J Phytoremediation. 2023 Aug 24;25(10):1269–88. doi:10.1080/15226514.2022.2147145 PubMed PMID: 36404648.
18. Bai RS, Abraham TE. Studies on chromium(VI) adsorption–desorption using immobilized fungal biomass. Bioresour Technol. 2003 Mar 1;87(1):17–26. doi:10.1016/S0960-8524(02)00222-5
19. Khare KS, Phelan FR. Quantitative Comparison of Atomistic Simulations with Experiment for a Cross-Linked Epoxy: A Specific Volume–Cooling Rate Analysis. Macromolecules. 2018 Jan 23;51(2):564–75. doi:10.1021/acs.macromol.7b01303
20. Ridha FN, Webley PA. Anomalous Henry's law behavior of nitrogen and carbon dioxide adsorption on alkali-exchanged chabazite zeolites. Sep Purif Technol. 2009;67(3):336–43. doi:10.1016/j.seppur.2009.03.045
21. Langmuir I. THE ADSORPTION OF GASES ON PLANE SURFACES OF GLASS, MICA AND PLATINUM. J Am Chem Soc. 1918;40(2):1361–402. doi:10.1021/ja01269a066
22. Jovanović DS. Physical adsorption of gases - I: Isotherms for monolayer and multilayer adsorption. Kolloid-Z Amp Z Für Polym. 1969;235(1):1203–13. doi:10.1007/BF01542530
23. Carmo AM, Hundal LS, Thompson ML. Sorption of hydrophobic organic compounds by soil materials: Application of unit equivalent Freundlich coefficients. Environ Sci Technol. 2000;34(20):4363–9. doi:10.1021/es000968v
24. Radushkevich LV. Potential theory of sorption and structure of carbons. Zhurnal Fiz Khimii. 1949;23:1410–20.
25. Dubinin MM. Modern state of the theory of volume filling of micropore adsorbents during adsorption of gases and steams on carbon adsorbents. Zh Fiz Khim. 1965;39(6):1305–17.
26. Mahanty B, Behera SK, Sahoo NK. Misinterpretation of Dubinin–Radushkevich isotherm and its implications on adsorption parameter estimates. Sep Sci Technol. 2023 May 3;58(7):1275–82. doi:10.1080/01496395.2023.2189050
27. Mudhoo A, Pittman CU. The Dubinin-Radushkevich models: Dissecting the *ps*/*p* to *cs*/*c*e replacement in solid-aqueous interfacial adsorption and tracking the validity of $E = 8$ kJ mol–1 for assigning sorption type. Chem Eng Res Des. 2023 Oct 1;198:370–402. doi:10.1016/j.cherd.2023.09.020
28. Koble RA, Corrigan TE. Adsorption isotherms for pure hydrocarbons. Ind Eng Chem. 1952 Feb 1;44(2):383–7. doi:10.1021/ie50506a049
29. Temkin MI, Pyzhev V. Kinetics of ammonia synthesis on promoted iron catalysts. Acta Physicochim USSR. 1940;12(3):327–56.
30. Chu KH. Revisiting the Temkin Isotherm: Dimensional Inconsistency and Approximate Forms. Ind Eng Chem Res. 2021 Aug 16. Located at: world. doi:10.1021/acs.iecr.1c01788
31. Redlich O, Peterson DL. A Useful Adsorption Isotherm. Shell Dev Co Emeryv Calif. 1958;63:1024.
32. Sips R. On the structure of a catalyst surface. J Chem Phys. 1948;16(5):490–5. doi:10.1063/1.1746922
33. Tóth J. Uniform interpretation of gas/solid adsorption. Adv Colloid Interface Sci. 1995;55(C):1–239. doi:10.1016/0001-8686(94)00226-3
34. Hill AV. The possible effects of the aggregation of the molecules of haemoglobin on its dissociation curves. J Physiol. 1910;40:iv–vii. doi:https://doi.org/10.1098/rspb.1936.0046
35. Brunauer S, Emmett PH, Teller E. Adsorption of Gases in Multimolecular Layers. J Am Chem Soc. 1938;60(2):309–19. doi:10.1021/ja01269a023
36. Vieth WR, Sladek KJ. A model for diffusion in a glassy polymer. J Colloid Sci. 1965;20(9):1014–33. doi:10.1016/0095-8522(65)90071-1
37. Brouers F, Sotolongo O, Marquez F, Pirard JP. Microporous and heterogeneous surface adsorption isotherms arising from Levy distributions. Phys Stat Mech Its Appl. 2005 Apr 1;349(1):271–82. doi:10.1016/j.physa.2004.10.032
38. Hamissa AMB, Brouers F, Mahjoub B, Seffen M. Adsorption of Textile Dyes Using Agave Americana (L.) Fibres: Equilibrium and Kinetics Modelling. Adsorpt Sci Technol. 2007 Jun 1;25(5):311–25. doi:10.1260/026361707783432533
39. Brouers F, Al-Musawi TJ. Brouers-Sotolongo fractal kinetics versus fractional derivative kinetics: A new strategy to analyze the pollutants sorption kinetics in porous materials. J Hazard Mater. 2018 May 15;350:162–8. doi:10.1016/j.jhazmat.2018.02.015
40. Fritz W, Schluender EU. Simultaneous adsorption equilibria of organic solutes in dilute aqueous solutions on activated carbon. Chem Eng Sci. 1974;29(5):1279–82. doi:10.1016/0009-2509(74)80128-4
41. Chu KH, Tan B. Is the Frumkin (Fowler–Guggenheim) adsorption isotherm a two- or three-parameter equation? Colloid Interface Sci Commun. 2021 Nov 1;45:100519. doi:10.1016/j.colcom.2021.100519
42. Martucci A, Braschi I, Bisio C, Sarti E, Rodeghero E, Bagatin R, et al. Influence of water on the retention of methyl tertiary-butyl ether by high silica ZSM-5 and Y zeolites: A multidisciplinary study on the adsorption from liquid and gas phase. RSC Adv. 2015;5(106):86997–7006.
43. Chu KH, Debord J, Harel M, Bollinger JC. Mirror, Mirror on the Wall, Which Is the Fairest of Them All? Comparing the Hill, Sips, Koble–Corrigan, and Liu Adsorption Isotherms. Ind Eng Chem Res. 2022 May 18;61(19):6781–90. doi:10.1021/acs.iecr.2c00507
44. Shukor MY. Chitosan–Silica Composite Aerogel for the Adsorption of Cupric Ions: Isothermal Remodeling and MOORA-Based Model Selection. J Environ Microbiol Toxicol. 2024 Dec 26;12(2):2. doi:10.54987/jemat.v12i2.1026
45. Akaike H. Factor analysis and AIC. Psychometrika. 1987;52(3):317–32. doi:10.1007/BF02294359
46. Burnham KP, Anderson DR. Model Selection and Multimodel Inference: A Practical Information-Theoretic Approach. Springer Science & Business Media; 2002. 528 p.
47. Ezekiel M. The Sampling Variability of Linear and Curvilinear Regressions: A First Approximation to the Reliability of the Results Secured by the Graphic "Successive Approximation" Method. Ann Math Stat. 1930;1(4):275–333. doi:https://doi.org/10.1214/aoms/1177733062
48. Ross T. Indices for performance evaluation of predictive models in food microbiology. J Appl Bacteriol. 1996;81(5):501–8.
49. Marquardt DW. An algorithm for least-squares estimation of nonlinear parameters. SIAM J Appl Math. 1963;11(2):431–41.
50. Seidel A, Gelbin D. On applying the ideal adsorbed solution theory to multicomponent adsorption equilibria of dissolved organic components on activated carbon. Chem Eng Sci. 1988 Jan 1;43(1):79–88. doi:10.1016/0009-2509(88)87128-8
51. Porter JF, McKay G, Choy KH. The prediction of sorption from a binary mixture of acidic dyes using single- and mixed-isotherm variants of the ideal adsorbed solute theory. Chem Eng Sci. 1999;54(24):5863–85. doi:10.1016/S0009-2509(99)00178-5
52. Schwarz G. Estimating the Dimension of a Model. Ann Stat. 1978;6(2):461–4.
53. Motulsky HJ, Ransnas LA. Fitting curves to data using nonlinear regression: a practical and nonmathematical review. FASEB J Off

Publ Fed Am Soc Exp Biol. 1987;1(5):365–74. doi:https://doi.org/10.1096/fasebj.1.5.3315805
54. Karel W, Brauers W, Zavadskas E. The MOORA method and its application to privatization in a transition economy. Control Cybern. 2006 Jan 1;35.
55. Brauers W. Multi-objective seaport planning by MOORA decision making. Ann Oper Res. 2013 Jul 1;206. doi:10.1007/s10479-013-1314-7
56. Gupta A, Gupta N, Garg R, Kumar R. Evaluation, Selection and Ranking of Software Reliability Growth Models using Multi criteria Decision making Approach. In: 2018 4th International Conference on Computing Communication and Automation (ICCCA) [Internet]. 2018 [cited 2025 Feb 18]. p. 1–8. Available from: https://ieeexplore.ieee.org/abstract/document/8777644 doi:10.1109/CCAA.2018.8777644
57. Lambert RJW, Mytilinaios I, Maitland L, Brown AM. Monte Carlo simulation of parameter confidence intervals for non-linear regression analysis of biological data using Microsoft Excel. Comput Methods Programs Biomed. 2012 Aug 1;107(2):155–63. doi:10.1016/j.cmpb.2011.05.009
58. Wu Z, Joo H, Ahn IS, Haam S, Kim JH, Lee K. Organic dye adsorption on mesoporous hybrid gels. Chem Eng J. 2004 Sep 15;102(3):277–82. doi:10.1016/j.cej.2004.05.008
59. Chandra IK, Ju YH, Ayucitra A, Ismadji S. Evans blue removal from wastewater by rarasaponin-bentonite. Int J Environ Sci Technol. 2013;10(2):359–70. doi:10.1007/s13762-012-0114-y
60. Vijayaraghavan K, Yun YS. Biosorption of C.I. Reactive Black 5 from aqueous solution using acid-treated biomass of brown seaweed Laminaria sp. Dyes Pigments. 2008 Jan 1;76(3):726–32. doi:10.1016/j.dyepig.2007.01.013
61. Foo KY, Hameed BH. Insights into the modeling of adsorption isotherm systems. Chem Eng J. 2010;156(1):2–10. doi:10.1016/j.cej.2009.09.013
62. Belhachemi M, Addoun F. Comparative adsorption isotherms and modeling of methylene blue onto activated carbons. Appl Water Sci. 2011 Dec 1;1(3):111–7. doi:10.1007/s13201-011-0014-1
63. Sivarajasekar N, Baskar R. Adsorption of basic red 9 onto activated carbon derived from immature cotton seeds: isotherm studies and error analysis. Desalination Water Treat. 2014 Dec 6;52(40–42):7743–65. doi:10.1080/19443994.2013.834518
64. Ayawei N, Ebelegi AN, Wankasi D. Modelling and Interpretation of Adsorption Isotherms. J Chem. 2017 Sep 5;2017:e3039817. doi:10.1155/2017/3039817
65. Maaloul N, Oulego P, Rendueles M, Ghorbal A, Díaz M. Cu(II) Ions Removal on Functionalized Cellulose Beads from Tunisian Almond (Prunus dulcis) Shell. Environ Sci Eng. 2021;65–71. doi:10.1007/978-3-030-51210-1_11
66. Chu KH, Hashim M, Santos YTDC, Debord J, Harel M, Bollinger JC. The Redlich–Peterson isotherm for aqueous phase adsorption: Pitfalls in data analysis and interpretation. Chem Eng Sci. 2023 Nov 28;285:119573. doi:10.1016/j.ces.2023.119573
67. Langmuir I. The constitution and fundamental properties of solids and liquids. Part I. Solids. J Am Chem Soc. 1916;38(11):2221–95. doi:10.1021/ja02268a002
68. Hyder AHMG, Begum SA, Egiebor NO. Adsorption isotherm and kinetic studies of hexavalent chromium removal from aqueous solution onto bone char. J Environ Chem Eng. 2015;3(2):1329–36. doi:10.1016/j.jece.2014.12.005
69. Divband Hafshejani L, Mortazavi P, Sabz ALiPour S, Brooman Nasab S. Isotherm and Kinetics Study of The Adsorption of Chromium (VI) From Aqueous Solution by Zizyphus Spina-christi Leaves Ash Nanoparticles. Irrig Sci Eng. 2016 Dec 21;39(4):97–110. doi:10.22055/jise.2016.12499
70. Taha AA, Shreadah MA, Ahmed AM, Heiba HF. Multi-component adsorption of Pb(II), Cd(II), and Ni(II) onto Egyptian Na-activated bentonite; Equilibrium, kinetics, thermodynamics, and application for seawater desalination. J Environ Chem Eng. 2016;4(1):1166–80. doi:10.1016/j.jece.2016.01.025
71. Nag S, Mondal A, Bar N, Das SK. Biosorption of chromium (VI) from aqueous solutions and ANN modelling. Environ Sci Pollut Res. 2017 Aug 1;24(23):18817–35. doi:10.1007/s11356-017-9325-6
72. Srivastava S, Agrawal SB, Mondal MK. Synthesis, characterization and application of Lagerstroemia speciosa embedded magnetic nanoparticle for Cr(VI) adsorption from aqueous solution. J Environ Sci China. 2017 May;55:283–93. doi:10.1016/j.jes.2016.08.012 PubMed PMID: 28477823.
73. Ahsan MdA, Jabbari V, Islam MdT, Kim H, Hernandez-Viezcas JA, Lin Y, et al. Green synthesis of a highly efficient biosorbent for organic, pharmaceutical, and heavy metal pollutants removal: Engineering surface chemistry of polymeric biomass of spent coffee waste. J Water Process Eng. 2018 Oct 1;25:309–19. doi:10.1016/j.jwpe.2018.08.005
74. Boeykens SP, Saralegui A, Caracciolo N, Piol MN. Agroindustrial waste for lead and chromium biosorption. J Sustain Dev Energy Water Environ Syst. 2018;6(2):341–50. doi:10.13044/j.sdewes.d5.0184
75. Mahmood-Ul-Hassan M, Suthar V, Ahmad R, Yousra M. Biosorption of metal ions on lignocellulosic materials: batch and continuous-flow process studies. Environ Monit Assess. 2018;190(5). doi:10.1007/s10661-018-6674-7
76. Mortazavian S, An H, Chun D, Moon J. Activated carbon impregnated by zero-valent iron nanoparticles (AC/nZVI) optimized for simultaneous adsorption and reduction of aqueous hexavalent chromium: Material characterizations and kinetic studies. Chem Eng J. 2018 Jul 1;353. doi:10.1016/j.cej.2018.07.170
77. Sadiq A, Choubey A, Bajpai AK, Sadiq A, Choubey A, Bajpai AK. Biosorption of chromium ions by calcium alginate nanoparticles. J Chil Chem Soc. 2018;63(3):4077–81. doi:10.4067/s0717-97072018000304077
78. Abilio TE, Soares BC, José JC, Milani PA, Labuto G, Carrilho ENVM. Hexavalent chromium removal from water: adsorption properties of in natura and magnetic nanomodified sugarcane bagasse. Environ Sci Pollut Res. 2021;28(19):24816–29. doi:10.1007/s11356-020-11726-8
79. Dan-Iya BI, Shukor MY. Isothermal modelling of the adsorption of chromium onto calcium alginate nanoparticles. J Environ Microbiol Toxicol. 2021 Dec 31;9(2):2. doi:10.54987/jemat.v9i2.607
80. Mahmoud ME, El-Said GF, Ibrahim GAA, Elnashar AAS. Effective removal of hexavalent chromium from water by sustainable nano-scaled waste avocado seeds: adsorption isotherm, thermodynamics, kinetics, and error function. Biomass Convers Biorefinery. 2022;14(13):14725–43. doi:https://doi.org/10.1007/s13399-022-03619-2